Critical anisotropies of a geometrically frustrated triangular-lattice antiferromagnet

M. Swanson,[1,2] J. T. Haraldsen,[1] and R. S. Fishman[1]
[1]*Materials Science and Technology Division, Oak Ridge National Laboratory, Oak Ridge, Tennessee 37831, USA*
[2]*North Dakota State University, Fargo, North Dakota 58105, USA*

(Received 2 February 2009; revised manuscript received 13 April 2009; published 12 May 2009; corrected 13 May 2009)

This work examines the critical anisotropy required for the local stability of the collinear ground states of a geometrically frustrated triangular-lattice antiferromagnet (TLA). Using a Holstein-Primakoff expansion, we calculate the spin-wave frequencies for the one-, two-, three-, four-, and eight-sublattice (SL) ground states of a TLA with up to third neighbor interactions. Local stability requires that all spin-wave frequencies are real and positive. The two-, four-, and eight-SL phases break up into several regions where the critical anisotropy is a different function of the exchange parameters. We find that the critical anisotropy is a continuous function everywhere except across the two-SL/three-SL and three-SL/four-SL phase boundaries, where the three-SL phase has the higher critical anisotropy.

DOI: 10.1103/PhysRevB.79.184413 PACS number(s): 75.30.Ds, 75.50.Ee, 61.05.fg

I. INTRODUCTION

Geometrically frustrated systems exhibit many novel characteristics including noncollinear ground states and multiferroic properties.[1] One of the best realizations of a geometrically frustrated triangular-lattice antiferromagnet (TLA) is $CuFeO_2$, which contains stacked hexagonal planes of spin-5/2 Fe^{3+} ions. Accompanied by a phase transition from a collinear four-sublattice (SL) ground state to a noncollinear phase,[2–5] $CuFeO_2$ exhibits multiferroic properties above a critical magnetic field or above a critical concentration of nonmagnetic Al^{3+} impurities, which substitute for the Fe^{3+} ions.[6,7] Inelastic neutron-scattering experiments[8–10] on $CuFeO_2$ have reported a spin-wave (SW) gap of about 0.9 meV, which decreases with Al doping and may vanish[11] upon the appearance of multiferroic behavior. Similar behavior is produced in a model TLA as the anisotropy is reduced[12] and spin fluctuations about the four-SL collinear phase become stronger.

In this paper, we evaluate the critical anisotropies required for the local stability of the collinear magnetic phases in a model TLA with up to third nearest neighbors. As shown elsewhere,[13] the wave vector of the dominant SW instabilities of a collinear phase coincides with the dominant wave vector of the noncollinear phase that appears with decreasing anisotropy. Therefore, an analysis of the critical anisotropies and wave vectors of a frustrated TLA can provide useful information about the noncollinear phases that appear at small anisotropy.

The collinear ground states of a TLA with strong anisotropy were first obtained by Takagi and Mekata,[14] who examined an Ising model with interactions up to third nearest neighbors. The ground-state phase diagram consists of the five phases sketched in Fig. 1, where the energies of these five states are given in Table I. Using a Holstein-Primakoff (HP) expansion, we have calculated the SW frequencies and critical anisotropies for each of these phases.

The Hamiltonian for a TLA is given by

$$H = -\frac{1}{2}\sum_{i\neq j} J_{ij}\mathbf{S}_i\cdot\mathbf{S}_j - D\sum_i \mathbf{S}_{iz}^2, \tag{1}$$

where $\mathbf{S}_i$ is the local moment on site i and D is the single-ion anisotropy. Here, the exchange coupling J_{ij} between sites i and j is antiferromagnetic when $J_{ij}<0$. Employing a HP transformation, the spin operators are given by $S_{iz}=S-a_i^\dagger a_i$, $S_{i+}=\sqrt{2S}a_i$, and $S_{i-}=\sqrt{2S}a_i^\dagger$. Expanded about the classical limit in powers of $1/\sqrt{S}$, the Hamiltonian can be written as $H=E+H_1+H_2+\cdots$. The first-order term H_1 vanishes when the spin configuration minimizes the energy E. The second-order term H_2 provides the dynamics of noninteracting SWs. Higher-order terms $H_{n>2}$ reflect the interactions between SWs. They are unimportant at low temperature and for small

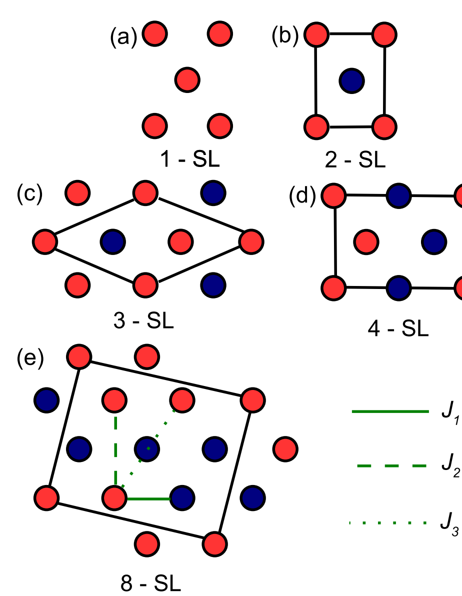

FIG. 1. (Color online) The one-, two-, three-, four-, and eight-SL phases for the ground states of the geometrically frustrated TLA. Solid black lines denote the magnetic unit cell of each phase. Up and down spins are designated by light red and dark blue circles, respectively.

TABLE I. Classical energies and critical anisotropies for TLA sublattices.

SL	Energy	$\mathbf{D}_c$
1-SL	$E^{(1)}/NS^2=-3J_1-3J_2-3J_3-D$	$D_c^{(1)}=0$
2-SL	$E^{(2)}/NS^2=J_1+J_2-3J_3-D$	$D_c^{(2\mathrm{I})}$ [Eq. (6)]
		$D_c^{(2\mathrm{II})}$ [Eq. (8)]
		$D_c^{(2\mathrm{III})}$ [Eq. (9)]
		$D_c^{(2\mathrm{IV})}=0$
3-SL	$E^{(3)}/NS^2=J_1-3J_2+J_3-D$	$D_c^{(3)}$ [Eq. (15)]
4-SL	$E^{(4)}/NS^2=J_1-J_2+J_3-D$	$D_c^{(4\mathrm{I})}$ [Eq. (18)]
		$D_c^{(4\mathrm{II})}$ [Eq. (19)]
8-SL	$E^{(8)}/NS^2=J_2+J_3-D$	$D_c^{(8\mathrm{I})}$ [Eq. (20)]
		$D_c^{(8\mathrm{II})}$ [Eq. (21)]

$1/S$. Similar to Takagi and Mekata,[14] we consider nearest-neighbor J_1, next-nearest-neighbor J_2, and next-next-nearest-neighbor J_3 exchange interactions, as sketched in Fig. 1. Whereas $J_1<0$ is always antiferromagnetic, J_2 and J_3 can be either positive or negative.

To determine the SW frequencies $\omega_{\mathbf{k}}$, we solve the equation of motion for the vectors $\mathbf{v}_{\mathbf{k}}=[a_{\mathbf{k}}^{(1)},a_{\mathbf{k}}^{(1)\dagger},a_{\mathbf{k}}^{(2)},a_{\mathbf{k}}^{(2)\dagger},\ldots]$, which may be written in terms of the $2N\times 2N$ matrix $\underline{M}(\mathbf{k})$ as $id\mathbf{v}_{\mathbf{k}}/dt=-[\underline{H}_2,\mathbf{v}_{\mathbf{k}}]=\underline{M}(\mathbf{k})\mathbf{v}_{\mathbf{k}}$, where N is the number of spin sites in the unit cell. The SW frequencies are then determined from the condition $\mathrm{Det}[\underline{M}(\mathbf{k})-\omega_{\mathbf{k}}\underline{I}]=0$.

Two conditions are required for the local stability of any magnetic phase: all SW frequencies must be real and positive and all SW weights must be positive. The SW weights $W_{\mathbf{k}}^{(s)}$ are coefficients of the spin-spin correlation function

$$S(\mathbf{k},\omega)=\frac{1}{N}\int dte^{-i\omega t}\sum_{i,j}e^{i\mathbf{k}\cdot\mathbf{d}_{ij}}\{\langle\mathbf{S}_i^+\mathbf{S}_j^-(t)\rangle+\langle\mathbf{S}_i^-\mathbf{S}_j^+(t)\rangle\}$$
$$=\sum_s W_{\mathbf{k}}^{(s)}\delta(\omega-\omega_{\mathbf{k}}^{(s)}),\tag{2}$$

where s denotes a branch of the SW spectrum and $\mathbf{d}_{ij}$ is defined as the vector pointing from site i to site j. The weights $W_{\mathbf{k}}^{(s)}$ were evaluated within the HP formalism by solving the equations of motion for coupled spin Green's functions.[15,16] In zero field, the condition that the SW weights are positive for all $\mathbf{k}$ is equivalent to the condition that all SW frequencies are positive.

We obtained analytic expressions for the SW frequencies for all phases shown in Fig. 1 with the exception of the eight-SL phase, which was solved numerically. Analysis of the SW frequencies yields the critical anisotropy D_c and the critical wave vectors $\mathbf{k}$, where the SW frequencies vanish. To simplify the following discussion, the SW and anisotropy coefficients are provided in the Appendix.

II. ONE-SUBLATTICE PHASE

The one-SL phase [Fig. 1(a)] is a ferromagnet with SW frequencies

$$\omega_{\mathbf{k}}^{(1)}=2S(D+A_{1\mathbf{k}}).\tag{3}$$

Since the one-SL phase is locally stable for any positive value of the anisotropy, $D_c=0$. The SW intensity $W_{\mathbf{k}}^{(1)}$ is constant throughout $\mathbf{k}$ for all interactions.

III. TWO-SUBLATTICE PHASE

For the two-SL phase [shown in Fig. 1(b)], the SW frequencies are given by

$$\omega_{\mathbf{k}}^{(2)}=2S\sqrt{A_{2\mathbf{k}}^2-A_{3\mathbf{k}}^2}.\tag{4}$$

The SW weights for the two-SL phase are

$$W_{\mathbf{k}}^{(2)}=\sqrt{\frac{A_{2\mathbf{k}}+A_{3\mathbf{k}}}{A_{2\mathbf{k}}-A_{3\mathbf{k}}}}.\tag{5}$$

From Eq. (4), the condition for the local stability of a two-SL phase is $A_{2\mathbf{k}}^2-A_{3\mathbf{k}}^2>0$. At D_c, $A_{2\mathbf{k}}^2=A_{3\mathbf{k}}^2$. This condition is satisfied when $D_c=0$ in most of the two-SL phase. But approaching the three-, four-, and eight-SL phase boundaries, nonzero anisotropy is required for local stability. As shown in Fig. 2(a), the critical anisotropy is continuous across the four-SL and eight-SL boundaries but is discontinuous across the three-SL boundary.

Upon closer examination [Fig. 2(c)], we find that D_c depends differently on the exchange parameters in the three regions designated by roman numerals. In region 2I [bounded by $J_3=J_2/2$, $J_3=(9J_2-J_1)/12$, and $J_3=J_2^2/(J_1-2J_2)$],

$$D_c^{(2\mathrm{I})}=\frac{1}{(4J_3)^3}\{-272J_3^4+64J_3^3J_2+48J_3^3J_1+72J_3^2J_2^2-48J_3^2J_2J_1$$
$$-8J_3^2J_1^2+36J_3J_2^2J_1-27J_2^4-(2J_3-J_2)C^3\},\tag{6}$$

where

$$C=\sqrt{(2J_3+3J_2)^2-8J_3J_1}.\tag{7}$$

In region 2II [bounded by $J_3=J_2/2$, $J_3=J_2$, $J_3=(8J_2-J_1)/9$, and $J_3=J_2^2/(J_1-2J_2)$],

$$D_c^{(2\mathrm{II})}=4J_2-\frac{9}{2}J_3-\frac{1}{2}J_1.\tag{8}$$

Finally, in region 2III [bounded by $J_3=J_2/2$, $J_3=J_1/4$, and $J_3=(J_1-J_2)/4$],

$$D_c^{(2\mathrm{III})}=-\frac{(4J_3+J_2-J_1)^2}{2(J_2+2J_3)}.\tag{9}$$

The critical wave vectors, $\mathbf{k}$, for the SW instabilities in region 2I are

$$k_x^{(2\mathrm{I},a)}a=2\arccos\left\{\frac{3J_2-2J_3-C}{8J_3}\right\},$$

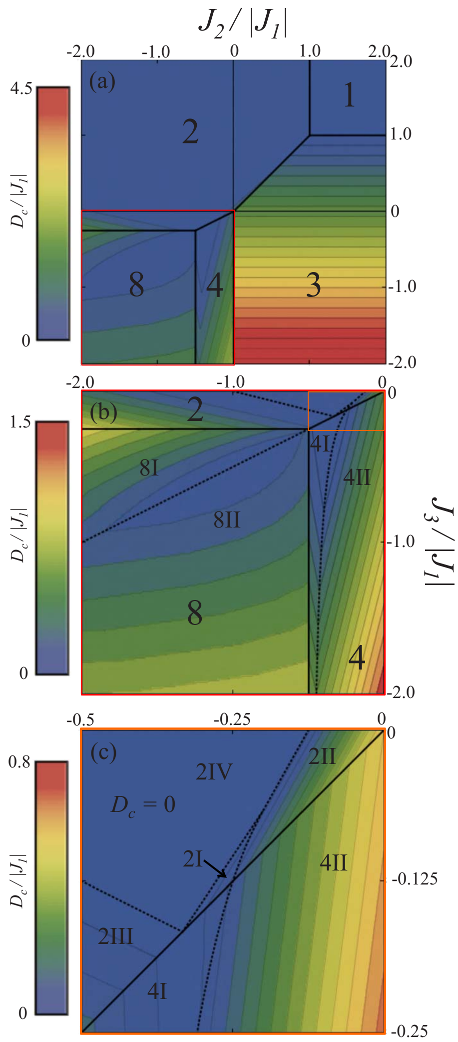

FIG. 2. (Color online) Critical anisotropies for the TLA ground states. The spacings between contours are (a) 0.2, (b) 0.1, and (c) 0.05. Numbers designate the stable phases and roman numerals designate regions where the behavior of the critical anisotropy is distinct. Solid lines denote boundaries between phases and dashed lines denote boundaries between regions. D_c is continuous across each phase boundary except for the two-SL/three-SL and the three-SL/four-SL phase boundaries; in both cases, D_c is higher for the three-SL phase. Note that each panel has a different scaling as shown on the left.

$$k_y^{(2\mathrm{I},a)}a=0. \tag{10}$$

Two other instabilities $\mathbf{k}^{(2\mathrm{I},b)}$ and $\mathbf{k}^{(2\mathrm{I},c)}$ are related to $\mathbf{k}^{(2\mathrm{I},a)}$ by $\pm\pi/3$ rotations and can be considered twins of the $\mathbf{k}^{(2\mathrm{I},a)}$ instabilities. All three instabilities occur at the same critical anisotropy $D_c^{(2\mathrm{I})}$. For regions 2II and 2III, the SW instabilities occur at

$$k_x^{(2\mathrm{II})}a=\pi\pm\pi/3,$$

$$k_y^{(2\mathrm{II})}a=0 \tag{11}$$

and

$$k_x^{(2\mathrm{III})}a=0,$$

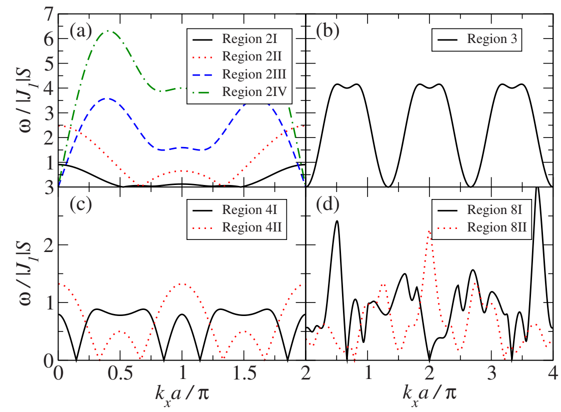

FIG. 3. (Color online) SW frequencies at the critical anisotropy for (a) two-, (b) three-, (c) four-, and (d) eight-SL phases (interaction parameters given in the text). All SW instabilities occur for $k_ya=0$ except in regions 2III and 8I, where they occur for $k_ya=0.186\pi$ and 0.382π, respectively.

$$k_y^{(2\mathrm{III})}a=\frac{2}{\sqrt{3}}\arccos\left\{\frac{J_2+J_1}{2(J_2+2J_3)}\right\} \tag{12}$$

along the k_x and k_y axes, respectively. Region 2IV is bounded by $J_2=0$, $J_3=(8J_2-J_1)/9$, and $J_3=(J_1-J_2)/4$ as shown in Figs. 2(b) and 2(c). This region has no critical anisotropy $D_c^{(2\mathrm{IV})}$ and is therefore a stable collinear phase for all $D\geq 0$.

Figure 3(a) shows three representative SWs for all two-SL regions. The interaction parameters for region 2I are $J_2/|J_1|=-0.25$, $J_3/|J_1|=-0.12$, and $D_c/|J_1|=0.04$. For region 2II, $J_2/|J_1|=-0.10$, $J_3/|J_1|=-0.05$, and $D_c/|J_1|=0.325$. For region 2III, $J_2/|J_1|=-0.75$, $J_3/|J_1|=-0.125$, and $D_c/|J_1|=0.031$. Finally, for region 2IV, the interaction parameters are $J_2/|J_1|=-1.0$, $J_3/|J_1|=-0.125$, and $D_c/|J_1|=0.0$. Regions I, II, and IV were evaluated with $k_ya=0$ while region III was evaluated at $k_ya=0.186\pi$ as explained above.

In Figs. 2(b) and 2(c), we examine the critical anisotropy of the two-SL phase along the $J_3/|J_1|=0$ axis. The critical anisotropy vanishes for $-1<J_2/|J_1|<-1/8$ but is nonzero outside this region. Therefore, noncollinear phases should appear for $J_2/|J_1|<-1$ and $J_2/|J_1|>-1/8$ when $D<D_c$. This agrees with Jolicoeur *et al.*,[17] who studied a TLA with nearest and next-nearest-neighbor exchange interactions and $D=0$. They obtain a Néel state up to $J_2/|J_1|=-1/8$ and an incommensurate spiral for $J_2/|J_1|<-1$. Similar results have been obtained on square lattices.[18,19]

IV. THREE-SUBLATTICE PHASE

For the three-SL phase [shown in Fig. 1(c)], the SW frequencies are

$$\omega_{\mathbf{k}}^{(3)}=6S\sqrt{R_{1\mathbf{k}}}\cos(\theta/3+2m/3\pi)+R_{2\mathbf{k}}/3, \tag{13}$$

where m is an integer (0,1,2) distinguishing the three separate SW dispersion relations and

$$\theta = \arccos\left\{\frac{2R_{2\mathbf{k}}^3 - 9R_{2\mathbf{k}}R_{3\mathbf{k}} - 27R_{4\mathbf{k}}}{1458R_{1\mathbf{k}}^{3/2}}\right\}. \quad (14)$$

The critical anisotropy of the three-SL phase is independent of J_2 and given by

$$D_c^{(3)} = -\frac{3}{2}(J_1 + J_3). \quad (15)$$

Notice that $D_c^{(3)}=0$ along the three-SL/one-SL boundary. Again, D_c is discontinuous along the two-SL/three-SL and three-SL/four-SL boundaries: the anisotropy required for the local stability of the three-SL phase is 3 times the critical anisotropy of the two- or four-SL phases. As discussed further below, the discontinuities at the two-SL/three-SL and three-SL/four-SL phase boundaries are related to the distinction between the conditions for global and local stabilities.

In Fig. 3(b), we plot a SW dispersion in the three-SL phase with interaction parameters $J_2/|J_1|=0.5$, $J_3/|J_1|=-0.5$, and $D_c/|J_1|=2.25$. Since the three-SL phase has a net moment, the SW frequencies are quadratic functions of $\mathbf{k}$ near the instability wave vectors.

V. FOUR-SUBLATTICE PHASE

The SW frequencies for the four-SL phase [shown in Fig. 1(d)] were evaluated in Ref. 12 and are given by

$$\omega_{\mathbf{k}}^{(4)} = 2S(A_{6\mathbf{k}}^2 - A_{7\mathbf{k}}^2 \pm [(F_{2\mathbf{k}}^2 - F_{2\mathbf{k}}^{*2})^2 + 4|A_{6\mathbf{k}}F_{2\mathbf{k}} - A_{7\mathbf{k}}F_{2\mathbf{k}}^*|^2]^{1/2})^{1/2}. \quad (16)$$

The SW weights of the four-SL phase are

$$W_{\mathbf{k}}^{(4)} = [R_{5\mathbf{k}}(A_{7\mathbf{k}} - A_{6\mathbf{k}}) + (F_{2\mathbf{k}} + F_{2\mathbf{k}}^*)(A_{6\mathbf{k}} - A_{7\mathbf{k}})^2 + (F_{2\mathbf{k}} - F_{2\mathbf{k}}^*)^2(F_{2\mathbf{k}} + F_{2\mathbf{k}}^* - A_{6\mathbf{k}} - A_{7\mathbf{k}})] \times [R_{5\mathbf{k}}\sqrt{A_{6\mathbf{k}}^2 - A_{7\mathbf{k}}^2} - R_{5\mathbf{k}}]^{-1}. \quad (17)$$

As for the two-SL phase, the critical anisotropy D_c for the four-SL phase depends differently on the interaction parameters in two regions, again denoted by roman numerals I and II [Fig. 2(b)]. In region 4I [bounded by $J_3=J_2/2$, $J_2=J_1/2$, and $J_3=J_2^2/(J_1-2J_2)$],

$$D_c^{(4\mathrm{I})} = \frac{1}{(4J_3)^3}\{-16J_3^4 - 64J_3^3J_2 + 48J_3^3J_1 + 72J_2^2J_3^2 - 8J_3^2J_1^2 - 48J_3^2J_2J_1 + 36J_3J_2^2J_1 - 27J_2^4 + (2J_3 - J_2)C^3\}, \quad (18)$$

and in region 4II [bounded by $J_3=J_2/2$, $J_2=0$, and $J_3=J_2^2/(J_1-2J_2)$],

$$D_c^{(4\mathrm{II})} = 2J_2 - \frac{1}{2}J_3 - \frac{1}{2}J_1. \quad (19)$$

The critical wave vectors for the four-SL phase are the same as those in the respective region of the two-SL phase, including the multiple instabilities in region 2I: $\mathbf{k}^{(4\mathrm{I},a)}=\mathbf{k}^{(2\mathrm{I},\mathrm{a})}$, $\mathbf{k}^{(4\mathrm{I},b)}=\mathbf{k}^{(2\mathrm{I},b)}$, and $\mathbf{k}^{(4\mathrm{II})}=\mathbf{k}^{(2\mathrm{II})}$. Figure 3(c) shows two representative SWs for regions 4I and 4II with $k_ya=0$. The interaction parameters for region 4I are $J_2/|J_1|=-0.439$, $J_3/|J_1|=-0.570$, and $D_c/|J_1|=0.105$. For region 4II, they are $J_2/|J_1|=-0.25$, $J_3/|J_1|=-0.5$, and $D_c/|J_1|=0.25$.

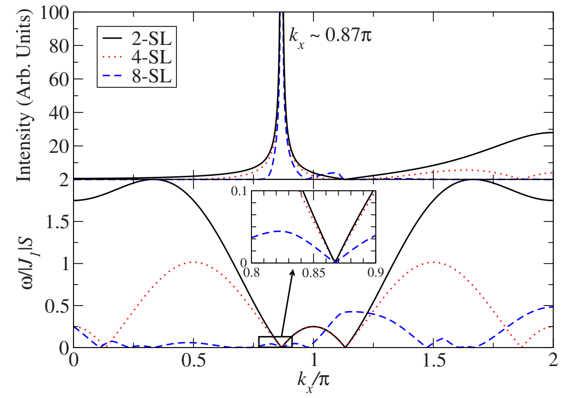

FIG. 4. (Color online) SW frequencies and SF intensities for the two-, four-, and eight-SL phases at the critical anisotropy with $J_2/|J_1|=-0.5$, $J_3/|J_1|=-0.25$, and $D/|J_1|=0.125$.

Figure 4 shows the SW frequencies and SF intensities for the two-, four-, and eight-SL phases at the triple point of the phase diagram. The intensities for the eight-SL phase were determined numerically. As shown in Fig. 4, each phase becomes unstable at $D/|J_1|=0.125$, where the SW intensity for each phase peaks at the same wave vector. This wave vector corresponds to the ordering wave vector of the noncollinear phase[13] that appears at small anisotropy. Because the two-, four-, and eight-SL phases all have zero net moments, their SW frequencies are linear functions of $\mathbf{k}$ around the wave vectors of the instabilities.

The four-SL phase is of particular interest since it is the known ground state[2] of $CuFeO_2$. Fits of the experimental SW frequencies[8,15] of $CuFeO_2$ have determined the ratios of exchange parameters $J_2/|J_1|\approx-0.44$ and $J_3/|J_1|\approx-0.57$, which lies within region 4I. Consequently, we have studied the SW frequencies of the four-SL phase more closely. Figure 5 shows the behavior of $k_x^{(4\mathrm{I},a)}$ along various cuts through region 4I of phase space. Since the SW frequencies are symmetric about the midpoint of the Brillouin zone $a\pi$, we consider the quantity $\Delta \equiv a|k_x-\pi|$. As $J_3/|J_1|$ increases in region 4I, Δ asymptotically approaches $\pi/3$, which is the constant value of Δ in region 4II. For small values of $J_3/|J_1|$, the wave-vector instabilities approach π as $J_2/|J_1|$ increases, equal π for $J_2/|J_1|=-1/3$, and then move away from π as $J_2/|J_1|$ approaches zero; this behavior is shown along the two-SL/four-SL boundary in Fig. 5(b).

VI. EIGHT-SUBLATTICE PHASE

For the eight-SL phase [shown in Fig. 1(e)], we have determined the SW dispersion relations numerically. The critical anisotropy values for this phase are shown in Fig. 2(a). Notice that D_c has a cusp dividing the phase into regions 8I and 8II [Fig. 2(b)], separated by $J_3=J_2/2$. Looking more closely at the numerical results, the critical anisotropies in the eight-SL regions are closely related to those of their respective neighbors and are given by

$$D_c^{(8\mathrm{I})} = D_c^{(2\mathrm{III})} + 4J_3 - J_1, \quad (20)$$

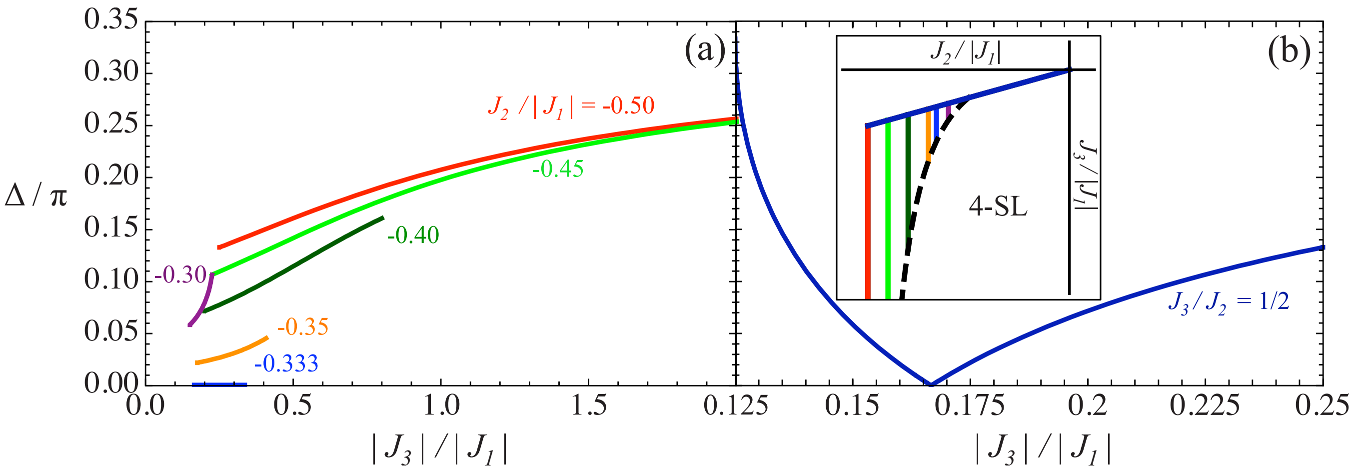

FIG. 5. (Color online) (a) Location of SW instability $\Delta = a|k_x - \pi|$ along $k_y a = 0$ in region 4I for fixed values of $J_2/|J_1|$. As $|J_3|/|J_1|$ increases along $J_2/|J_1| = -0.5$, Δ asymptotically approaches $\pi/3$. (b) Plot of Δ in region 4I along the two-SL/four-SL boundary $J_3/J_2 = 1/2$. The cusp in Δ occurs at $J_2/|J_1| = -1/3$ where the SW instability occurs at π.

$$D_c^{(8\text{II})} = D_c^{(4\text{I})} + 2J_2 - J_1, \tag{21}$$

which clearly show that the critical anisotropies are continuous across the phase boundaries. In region 8II, the wave-vector instabilities occur for $k_y = 0$ (as in region 4I); in region 8I, the wave-vector instabilities occur for nonzero k_y (as in region 2III). Figure 3(d) shows two representative SWs for regions 8I and 8II. The interaction parameters for region 8I are $J_2/|J_1| = -1.5$, $J_3/|J_1| = -0.50$, and $D_c/|J| = 0.25$. For region 8II, they are $J_2/|J_1| = -0.75$, $J_3/|J_1| = -0.50$, and $D_c/|J_1| = 0.62$. Whereas $k_y a = 0$ for region 8II and $k_y a = 0.382\pi$ for region 8I as explained above.

To better understand the discontinuities along the two-SL/three-SL and three-SL/four-SL phase boundaries, we consider the relationship between local and global stabilities. Our SW calculations only guarantee the local stability of each collinear phase. But even when a phase is locally stable, it can still be globally unstable to a lower-energy spin configuration. Hence, the critical anisotropy $\tilde{D}_c$ for global stability must be greater than or equal to the critical anisotropy D_c for local stability. Unlike D_c, $\tilde{D}_c$ must also be a continuous function of J_1, J_2, and J_3. So when D_c is discontinuous, the phase with the lower critical anisotropy cannot be globally stable. Since the three-SL phase has a higher critical anisotropy along the two- and four-SL boundaries, the two-SL and four-SL phases cannot be globally stable along those boundaries when $D_c^{(2\text{II})} < D < D_c^{(3)}$ or $D_c^{(4\text{II})} < D < D_c^{(3)}$. Therefore, our results for the local stability of the collinear phases also have implications for the global stability of those phases.

VII. CONCLUSION

We have examined the critical anisotropy for a geometrically frustrated TLA. Based on the Takagi-Mekata[14] phase diagram, we calculated the SW frequencies for all five phases. Imposing the two conditions for local stability, we obtained the critical anisotropies and wave-vector instabilities for all phases as functions of the exchange interactions. Surprisingly, these results are highly dependent on the longer-range exchange interactions and most phases break into several regions where the anisotropy has a distinct dependence on the exchange parameters. As discussed for the two-SL and four-SL phases, the critical anisotropies and wave vectors for the local stability of the collinear phases provide useful information about the noncollinear phases that appear at small anisotropy. We have also shown that the discontinuity of the critical anisotropy at the two-SL/three-SL and three-SL/four-SL phase boundaries has implications for the global stability of the two-SL and four-SL phases with the smaller critical anisotropies.

It is expected that this investigation of the collinear phases of the TLA enables one to characterize the possible noncollinear phases at small anisotropy. An examination of the critical wave vectors for each collinear phase can provide useful information about the dominant ordering wave vector of the underlying noncollinear phase that may arise. We believe that an analysis similar to that performed in this paper can also provide useful information for a variety of other physically important frustrated systems.

ACKNOWLEDGMENTS

We would like to acknowledge helpful conversations with Gonzalo Alvarez. This research was sponsored by the Laboratory Directed Research and Development Program of Oak Ridge National Laboratory, managed by UT-Battelle, LLC for the U.S. Department of Energy under Contract No. DEAC05-00OR22725 and by the Division of Materials Science. We would also like to acknowledge the DOE SULI program for support during this research.

APPENDIX: SPIN-WAVE AND ANISOTROPY COEFFICIENTS

This appendix provides the coefficients that enter the SW frequencies and weights for each phase. The coefficients for the one-SL or ferromagnetic phase are

$$A_{1\mathbf{k}} = 3(J_1 + J_2 + J_3) - J_1[\cos(\mathbf{k}\cdot\mathbf{d}_1) + \cos(\mathbf{k}\cdot\mathbf{d}_2) + \cos(\mathbf{k}\cdot\mathbf{d}_3)] - J_2[\cos(\mathbf{k}\cdot\mathbf{d}_4) + \cos(\mathbf{k}\cdot\mathbf{d}_5) + \cos(\mathbf{k}\cdot\mathbf{d}_6)] - J_3[\cos(2\mathbf{k}\cdot\mathbf{d}_1) + \cos(2\mathbf{k}\cdot\mathbf{d}_2) + \cos(2\mathbf{k}\cdot\mathbf{d}_3)], \quad (A1)$$

where $\mathbf{d}_1 = a\mathbf{x}$, $\mathbf{d}_2 = 1/2a\mathbf{x} + \sqrt{3}/2a\mathbf{y}$, $\mathbf{d}_3 = -1/2a\mathbf{x} + \sqrt{3}/2a\mathbf{y}$, $\mathbf{d}_4 = 3/2a\mathbf{x} + \sqrt{3}/2a\mathbf{y}$, $\mathbf{d}_5 = \sqrt{3}a\mathbf{y}$, and $\mathbf{d}_6 = -3/2a\mathbf{x} + \sqrt{3}/2a\mathbf{y}$.

The two-SL phase coefficients are

$$A_{2\mathbf{k}} = D + 3J_3 - J_1(\cos(\mathbf{k}\cdot\mathbf{d}_1) + 1) - J_2(\cos(\mathbf{k}\cdot\mathbf{d}_5) + 1) - J_3(\cos(2\mathbf{k}\cdot\mathbf{d}_1) + \cos(2\mathbf{k}\cdot\mathbf{d}_2) + \cos(2\mathbf{k}\cdot\mathbf{d}_3)), \quad (A2)$$

$$A_{3\mathbf{k}} = J_1(\cos(\mathbf{k}\cdot\mathbf{d}_2) + \cos(\mathbf{k}\cdot\mathbf{d}_3)) + J_2(\cos(\mathbf{k}\cdot\mathbf{d}_4) + \cos(\mathbf{k}\cdot\mathbf{d}_6)). \quad (A3)$$

The three-SL phase coefficients are

$$R_{1\mathbf{k}} = R_{2\mathbf{k}}^2 - 3R_{3\mathbf{k}}, \quad (A4)$$

$$R_{2\mathbf{k}} = 2A_{4\mathbf{k}} + A_{5\mathbf{k}}, \quad (A5)$$

$$R_{3\mathbf{k}} = A_{4\mathbf{k}}^2 + 2A_{4\mathbf{k}}A_{5\mathbf{k}} + |F_{1\mathbf{k}}|^2, \quad (A6)$$

$$R_{4\mathbf{k}} = (A_{5\mathbf{k}} - 2A_{4\mathbf{k}})|F_{1\mathbf{k}}|^2 - A_{4\mathbf{k}}^2 A_{5\mathbf{k}} - F_{1\mathbf{k}}^3 - F_{1\mathbf{k}}^{*3}, \quad (A7)$$

$$A_{4\mathbf{k}} = 2D + 2J_2(3 - \cos(\mathbf{k}\cdot\mathbf{d}_4) - \cos(\mathbf{k}\cdot\mathbf{d}_5) - \cos(\mathbf{k}\cdot\mathbf{d}_6)), \quad (A8)$$

$$A_{5\mathbf{k}} = 6J_1 + 6J_3 - A_{3\mathbf{k}}, \quad (A9)$$

$$F_{1\mathbf{k}} = J_1(e^{-i\mathbf{k}\cdot\mathbf{d}_2} + e^{i\mathbf{k}\cdot\mathbf{d}_1} + e^{i\mathbf{k}\cdot\mathbf{d}_3}) + J_3(e^{2i\mathbf{k}\cdot\mathbf{d}_2} + e^{-2i\mathbf{k}\cdot\mathbf{d}_1} + e^{-2i\mathbf{k}\cdot\mathbf{d}_3}). \quad (A10)$$

As in Ref. 12, the four-SL phase coefficients are

$$R_{5\mathbf{k}} = (F_{2\mathbf{k}}^4 + F_{2\mathbf{k}}^{*4} - 2(F_{2\mathbf{k}}^{*2} + 2A_{6\mathbf{k}}A_{7\mathbf{k}})F_{2\mathbf{k}}^2 + 4(A_{6\mathbf{k}}^2 + A_{7\mathbf{k}}^2)|F_{2\mathbf{k}}|^2 - 4A_{6\mathbf{k}}A_{7\mathbf{k}}F_{2\mathbf{k}}^{*2})^{1/2}, \quad (A11)$$

$$A_{6\mathbf{k}} = D - J_1 + J_2(1 - \cos(\mathbf{k}\cdot\mathbf{d}_5) \; - J_3(1 + \cos(2\mathbf{k}\cdot\mathbf{d}_1)), \quad (A12)$$

$$A_{7\mathbf{k}} = -\cos(\mathbf{k}\cdot\mathbf{d}_1)(J_1 + 2J_3\cos(\sqrt{3}\mathbf{k}\cdot\mathbf{d}_5)), \quad (A13)$$

$$F_{2\mathbf{k}} = -\cos(\mathbf{k}\cdot\mathbf{d}_5/2)(J_1 e^{i\mathbf{k}\cdot\mathbf{d}_1/2} + J_2 e^{-3i\mathbf{k}\cdot\mathbf{d}_1/2}). \quad (A14)$$

[1] *Frustrated Spin Systems*, edited by H. T. Diep (World Scientific, Singapore, 2004).

[2] S. Mitsuda, H. Yoshizawa, N. Yaguchi, and M. Mekata, J. Phys. Soc. Jpn. **60**, 1885 (1991).

[3] M. Mekata, N. Yaguchi, T. Takagi, T. Sugino, S. Mitsuda, H. Yoshizawa, N. Hosoito, and T. Shinjo, J. Phys. Soc. Jpn. **62**, 4474 (1993).

[4] O. A. Petrenko, M. R. Lees, G. Balakrishnan, S. de Brion, and G. Chouteau, J. Phys.: Condens. Matter **17**, 2741 (2005).

[5] N. Terada, Y. Narumi, K. Katsumata, T. Yamamoto, U. Staub, K. Kindo, M. Hagiwara, Y. Tanaka, A. Kikkawa, H. Toyokawa, T. Fukui, R. Kanmuri, T. Ishikawa, and H. Kitamura, Phys. Rev. B **74**, 180404(R) (2006).

[6] N. Terada, S. Mitsuda, T. Fujii, K. Soejima, I. Doi, H. Aruga Katori, and Y. Noda, J. Phys. Soc. Jpn. **74**, 2604 (2005).

[7] S. Seki, Y. Yamasaki, Y. Shiomi, S. Iguchi, Y. Onose, and Y. Tokura, Phys. Rev. B **75**, 100403(R) (2007).

[8] F. Ye, J. A. Fernandez-Baca, R. S. Fishman, Y. Ren, H. J. Kang, Y. Qiu, and T. Kimura, Phys. Rev. Lett. **99**, 157201 (2007).

[9] N. Terada, S. Mitsuda, Y. Oohara, H. Yoshizawa, and H. Takei, J. Magn. Magn. Mater. **272-276**, e997 (2004).

[10] T. Kimura, J. C. Lashley, and A. P. Ramirez, Phys. Rev. B **73**, 220401(R) (2006).

[11] N. Terada, S. Mitsuda, T. Fujii, and D. Petitgrand, J. Phys.: Condens. Matter **19**, 145241 (2007).

[12] R. S. Fishman, J. Appl. Phys. **103**, 07B109 (2008).

[13] J. T. Haraldsen, M. Swanson, G. Alvarez, and R. S. Fishman, arXiv:0901.2336 (unpublished).

[14] T. Takagi and M. Mekata, J. Phys. Soc. Jpn. **64**, 4609 (1995).

[15] R. S. Fishman, F. Ye, J. A. Fernandez-Baca, J. T. Haraldsen, and T. Kimura, Phys. Rev. B **78**, 140407(R) (2008).

[16] J. T. Haraldsen and R. S. Fishman, J. Phys.: Condens. Matter **21**, 216001 (2009).

[17] Th. Jolicoeur, E. Dagotto, E. Gagliano, and S. Bacci, Phys. Rev. B **42**, 4800 (1990).

[18] E. Dagotto and A. Moreo, Phys. Rev. Lett. **63**, 2148 (1989).

[19] P. Chandra and B. Doucot, Phys. Rev. B **38**, 9335 (1988).